Imaging of nerve injury with HSP27 antibody-functionalized photoacoustic nanoprobes

Hongjiang Chen (陈洪江)[1], Zhongjiang Chen (陈重江)[2], Jankun Xu (许建坤)[1], and Jun Hu (胡 军)[1,2,*]

[1]*Department of Orthopaedics, the First Affiliated Hospital, Shantou University Medical College, Shantou 515041, China*

[2]*MOE Key Laboratory of Laser Life Science & Institute of Laser Life Science, College of Biophotonics, South China Normal University, Guangzhou 510631, China*

**Corresponding author: hjzkm@vip.163.com*

Received May 19, 2015; accepted August 28, 2015; posted online October 16, 2015

Early detection and timely treatment of nerve injury is crucial for the repair of nerve function. One week following a crush injury, heat shock protein 27 (HSP27) is over-expressed along the entire length of the sciatic nerve. Herein, we present an approach to detect injured nerves by photoacoustic microscopy after labeling the injured nerve with HSP27 antibody-conjugated gold nanoparticles. The studies reveal that nanoprobe administration enabled the detection of injured nerves by photoacoustic microscopy, especially during the early stages within 3–7 days post injury. In conclusion, photoacoustic microscopy combined with antibody-conjugated nanoparticles holds potential for the early detection of nerve injury.

OCIS codes: 170.0170, 170.3880, 170.5120.

doi: 10.3788/COL201513.111701.

Evidence suggests that injured nerves can achieve better functional recovery when treated in a timely manner[1]. Therefore, early diagnosis and appropriate treatment is very important in cases of nerve injury and would likely lead to better functional restoration. Electromyography (EMG) is the only approach that can detect injured motor or sensory nerves. However, EMG is invasive and only detects abnormalities at approximately 14–21 days after the injury occurred[2,3]. Since tissue and nerves possess early the same parameters of density and acoustic impedance, conventional methods, such as ultrasound imaging, X-rays, computed tomography (CT), and magnetic resonance imaging (MRI), cannot provide high contrast imaging sufficient for identifying injured nerves *in situ*[2,4,5]. Therefore, a novel and more effective technology for the early detection of nerve injury is urgently needed.

Advances in nanotechnology have identified promising candidates that are more suitable for biological and biomedical applications over a wide variety of disorders. Nanoparticles (NPs) with unique properties such as small particle size, novel physicochemical properties, and easy surface modification are widely used for biomedical purposes[6,7]. Targeting ligands, imaging labels, and therapeutic drugs could all be integrated with contrast reagents as a promising approach for targeted molecular imaging and therapy[8,9]. Due to the photoacoustic effect, photoacoustic microscopy is a noninvasive imaging modality with high resolution and high contrast[10–13]. It has been successfully applied to several biomedical applications for obtaining structural and functional information, including the detection of hemoglobin oxygen saturation and carboxyhemoglobin saturation, monitoring of vascular damage during photodynamic therapy treatment of tumors, noninvasive monitoring of traumatic brain injury, and post-traumatic rehabilitation[14–17]. Previous studies have shown that heat shock protein 27 (HSP27) in peripheral nerves can protect injured cells by preventing oxidative stress[18] and resisting heat shock[19]. Costigan *et al.* found that HSP27 was upregulated by 9-foldin the ipsilateral dorsal root ganglion (DRG) 48 h after axotomy of the sciatic nerve[20]. Hirata *et al.* also found that HSP27 localization extended from the proximal to the distal part of the axon and propagated through the entire nerve within one week after the surgery[21]. Therefore, due to the dramatic upregulation of HSP27 in injured neurons, we hypothesized that HSP27 could act as an effective marker for early nerve injury. Four-week-old Sprague–Dawley (SD) rats (male) weighing 80–100 g were used in the experiments. The rats were placed under general anesthesia with sodium pentobarbital (200 mg/kg, i.p.) and then the left sciatic nerve of the rat was crushed at the middle of the femur for 30 s with Jeweler's forceps. Control animals received the same surgical procedure but without crushing the nerve. Neurons were cultured according to the method previously described[20]. All procedures followed the rules of the National Animal Protection of China.

A diagram of the photoacoustic microscopy system is presented in Fig. 1. Briefly, a tunable pulsed laser source (Vibrant B 532I, Opotek, USA) with wavelengths of 532 and 680–960 nm, a pulse width of 10 ns, and a pulse repetition rate of 10 Hz, was used to provide optical illumination. The laser beam was focused by an objective lens through a small hole in the center of the hollow sensor and a photodiode was used to monitor and calibrate the beam intensity and stability. The cylindrical lens and the position sensor device (PSD) acted as an autofocusing

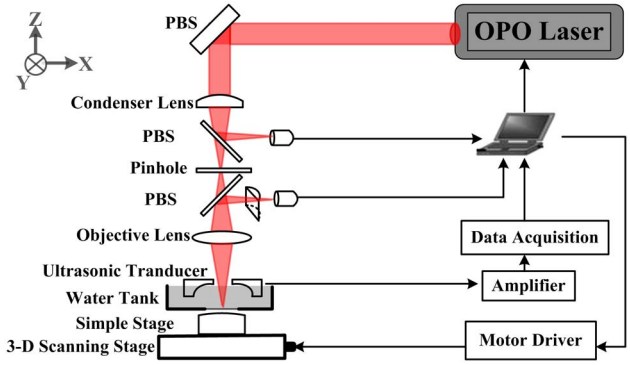

Fig. 1. Scheme of the photoacoustic microscopy system.

system. A dual-channel data acquisition card (NI 5224, National Instruments, USA) received the amplifier photoacoustic signals from the hollow sensor at a sampling rate of 200 M samples/s. At each sampling position, the photoacoustic signals were averaged 20 times. An X-Y-Z scanning stage was driven by computer-controlled stepper motors. Finally, the collected photoacoustic signals were reconstructed into images using the MATLAB program (MathWorks, Inc.).

In our study we found that HSP27 expression was induced in the injured sciatic nerves (Fig. 2). After the crushing injury, the expression level of HSP27 was significantly increased by approximately 28% and 60% at 3 and 7 days post trauma, respectively, as indicated by a western blot [Figs. 2(a) and 2(b)]. Therefore, HSP27 could serve as an indicator of early nerve injury.

The nanoprobes complex synthesis scheme is shown in Fig. 3. First, HS-PEG-COOH (heat shocked polyethylene glycol carboxylic acid) was immobilized on the surface of gold NP through the formation of stable, covalent gold-thiol linkages. The carboxylic terminal of the PEG was then conjugated to a wide range of biological molecules. Second, protein G was coupled to Au NPs-PEG-COOH through amino and carboxyl reactions after being

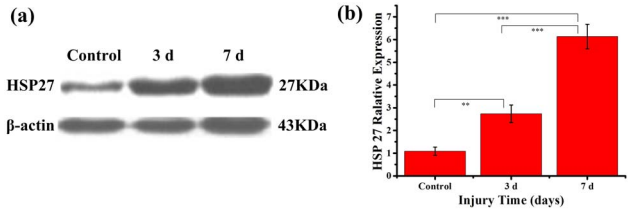

Fig. 2. Effect of trauma on the protein expression level of HSP27. (a) Western blot of HSP27 protein in the total lysate collected from the sciatic nerve of naive rats (control) and at 3 and 7 days after trauma (3d, 7d). The treatment induced a time-dependent increase in HSP27 protein levels. Note that the anti-HSP27 antibody recognized a band of 27 kDa in size. The expression of β-actin (43 kDa) was shown as a control for equal protein loading. (b) One-way ANOVA was used to compare differences between control and treated groups. Values of HSP27 protein levels were normalized to β-actin and the data were graphed as mean ± S.E.M. **, $p < 0.01$ and ***, $p < 0.001$.

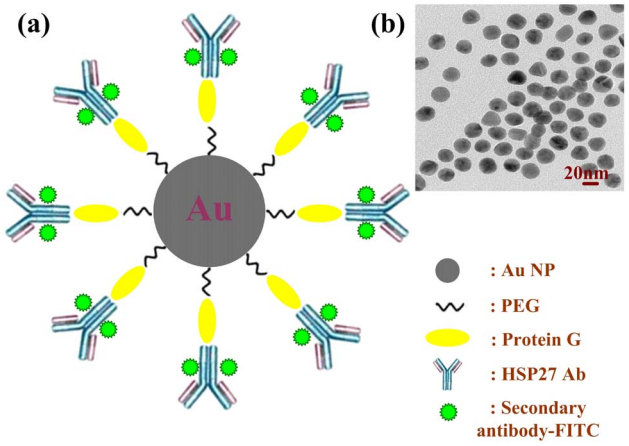

Fig. 3. Illustration of the nanotargeted probe. (a) The schematic diagram of Au NPs-HSP27Abs and the graphical symbols represent the components of Au NPs-HSP27Abs. (b) The insert is a TEM image of Au NPs with a scale bar of 20 nm.

activated with 1-Ethyl-3-(3-dimethylaminopropyl)-carbodiimide N-hydroxysuccinimide (EDC/NHS). To ensure that Au NPs-PEG-Protein G was bound to the Fc portion of the anti-HSP27 antibody, the functional regions (Fv) of the HSP27Ab for recognizing HSP27 were reserved. Finally, Au NPs-PEG-Protein G was conjugated to HSP27Ab-FITC to produce Au NPs-HSP27Abs-FITC.

Au NPs are particularly suitable for biological applications due to their photo-stability, water solubility, and lack of toxicity. Antibodies with high affinity and availability are widely used to establish biomarkers. Thiolated polyethylene glycol (PEG-SH) is used to attach Au NPs through a near-covalent gold-thiol bond in order to achieve a stable union. The PEG chains extend into the aqueous phase to impart solubility in water. Since the sheath of PEG can avoid clearance of Au NPs by the reticuloendothelial system, Au NPs functionalized with PEG have been shown to persist longer in circulation. Protein G acts as an intermediate conjugate between Au NPs-PEG and HSP27Ab. It can also be more easily conjugated to the Fc region compared to the Fab region. Moreover, using this conjugation strategy allows the Fab region of the anti-HSP27 antibody to specifically target HSP27. Moreover, the non-covalent interaction between SH-PEG and Au NPs resulted in the suspensions of Au NPs-HSP27Abs being highly soluble and stable in PBS without any visible aggregations for at least two weeks at 4°C.

Unbound HSP27Ab and secondary antibody-FITC were removed by centrifugation in the final complex of reaction reagents. To confirm the correct composition of the Au NPs-HSP27Abs, the optical absorbance and fluorescence characteristics were investigated, respectively. Figure 4(a) shows that the absorption peak of the free Au NPs occurred at 530 nm (black curve) and that of the Au NPs-HSP27Abs occurred at 533 nm (red curve). As shown in Fig. 4(b), an excitation wavelength of 488 nm resulted

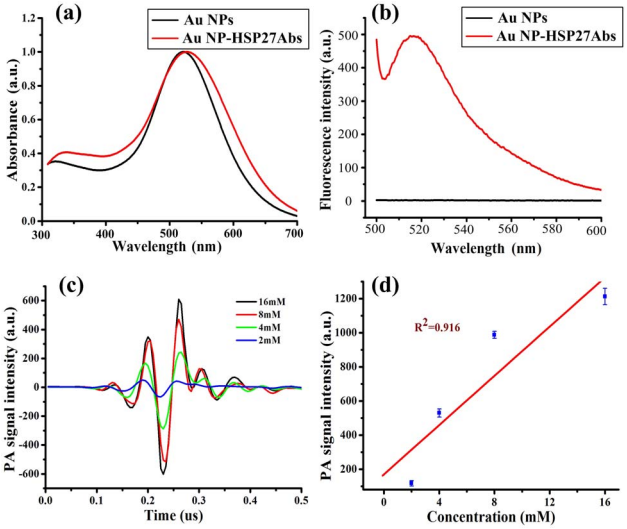

Fig. 4. (a) Absorbance spectra of Au NPs-HSP27Abs (red curve) and Au NPs (black curve) in PBS. (b) Fluorescence emission spectra of Au NPs-HSP27Abs (red curve) and Au NPs (black curve) in PBS with an excitation wavelength of 488 nm. (c) Photoacoustic signals of Au NPs-HSP27Abs at various Au NPs concentrations. (d) Linear fitting of photoacoustic signal intensity under the corresponding Au NPs concentrations.

in a fluorescence intensity of Au NPs-HSP27Abs that had a much stronger peak at 518 nm, but without the peak of fluorescence exhibited by Au NPs. The fluorescence peak of the Au NPs-HSP27Abs indicated that the HSP27Ab-FITC (FITC is fluorescein isothiocyanate) was well coupled with PEG-functionalized Au NPs.

To confirm whether Au NPs-HSP27Abs can be used as an ideal contrast agent for photoacoustic imaging, the concentration dependence of the photoacoustic signals generated by different concentrations of Au NPs-HSP27Abs was examined [Fig. 4(c)]. Briefly, 100 μL Au NPs-HSP27Abs with Au NP concentrations of 2, 4, 8, and 16 mmol/L were placed into a silicon tube with a diameter of 0.8 mm to determine their photoacoustic signals, respectively. As expected, the intensity of the photoacoustic signal linearly correlated to the gold concentrations [$R^2 = 0.916$, Fig. 4(d)]. Taken together, these results indicate that the Au NPs-HSP27Abs is an effective contrast agent for photoacoustic imaging.

Cells collected and divided into duplicate wells were exposed to the Au NPs (control group) and Au NPs-HSP27Abs (labeled group) (500 μL, gold concentration of 4 mmol/L) at 37°C. After incubation for 1 h, the free Au NPs and Au NPs-HSP27Abs in the cell cultures were removed by washing the plated cells twice with PBS. The cell suspensions were then injected into the hole of a cylindrical-shaped agar model for photoacoustic microscopy, respectively. The cylindrical-shaped agar model comprised of two 5-mm diameter holes that were each 2 mm deep. Unlabeled and labeled cell suspensions were injected into the holes of agar for photoacoustic microscopy with a 532 nm laser. Although the unconjugated Au NPs showed a weak signal, the Au NPs-HSP27Abs showed a much stronger signal compared to Au NPs in the injured neurons [Figs. 5(a) and 5(b)]. Therefore, the injured neurons can efficiently internalize the Au NPs-HSP27Abs nanotargeting probe.

We next performed an *in vitro* experiment to confirm the feasibility of using photoacoustic microscopy to detect a nerve injury with Au NPs-HSP27Abs as a contrast agent. Two nerves (1 cm in length) were incubated with Au NPs or Au NPs-HSP27Abs for 2 h at 4°C. In addition, an undamaged nerve was incubated with Au NPs-HSP27Abs under the same conditions. The nerves were arranged in parallel and embedded in a coupling agent on the agar phantom.

Heat shock proteins are a group of highly conserved proteins with important physiological functions in biological cells. Although HSP27 is weakly expressed in intact sciatic neurons, it can be induced by stressful stimuli and plays an important role in cell protection. We isolated HSP27 over expressing sciatic nerves 7 days after an acute injury. The injured nerve incubated with Au NPs-HSP27Abs showed a higher photoacoustic signal compared to the injured nerve incubated with Au NPs or the normal nerve incubated with Au NPs-HSP27Abs. Due to the ability of the nanotargeting probe to specifically bind to HSP27, the optical absorption of the injured nerve targeted with Au NPs-HSP27Abs (B) was much stronger than that of the injured nerve incubated with the Au NPs (A). In addition, compared to the normal nerve incubated with Au NPs-HSP27Abs (C), the injured nerve incubated with Au NPs-HSP27Abs also showed higher photoacoustic signal intensity. To quantify the targeting effect of the Au NPs-HSP27Abs probe, we determined the profile of intensities of the marked white dash line [Fig. 6(b)]. A comparison of signal intensities shows that the injured nerve targeted with Au NPs-HSP27Abs displayed a signal strength that was 2–3-fold above that of the uninjured nerve.

We investigated the feasibility of using photoacoustic microscopy for the early detection of nerve injury *in vivo*. The nontargeting Au NPs or targeting Au NP-HSP27Abs (100 μL, 8 mmol/L) were injected into the rat model in the left knee joint that the sciatic nerve was under the subcutaneous about 10 mm before imaging. Rats were

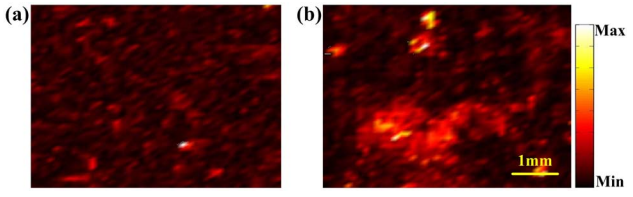

Fig. 5. Photoacoustic microscopy images of unlabeled and Au NPs-HSP27Abs-labeled neurons *in vitro*. (a) Photoacoustic microscopy image of neurons incubated with Au NPs. (b) Photoacoustic microscopy image of neurons labeled with Au NPs-HSP27Abs.

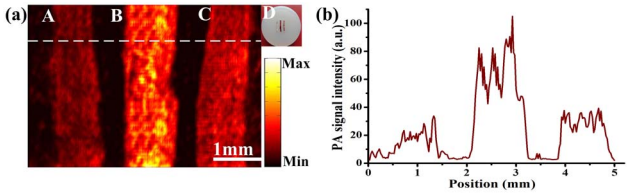

Fig. 6. Photoacoustic microscopy of normal and injured sciatic nerve using Au NPs and Au NPs-HSP27Abs as contrast agents. (a) Samples were arranged in parallel embedded in an agar phantom (D). Photoacoustic imaging of samples, including an injured nerve incubated with Au NPs (A), an injured nerve incubated with Au NPs-HSP27Abs (B), and a normal nerve incubated with Au NPs-HSP27Abs (C). (b) Photoacoustic microscopy signal intensity profiles extracted from the image along the horizontal white line running through the three nerve samples. The images of (a) were obtained by ultrasonic transducer array scanning with an excitation wavelength of 532 nm. The photoacoustic signal intensities of (b) correspond to the locations of the nerve being marked with a white line going through the three nerve sample in (a).

imaged by photoacoustic microscopy using a wavelength of 532 nm *in vivo* at 12 h after injection. The labeling of the injured sciatic nerve significantly increased and was spread over the entire nerve bundle. This is consistent with previous studies where we found that normal nerves were undetectable by photoacoustic microscopy. However, after the HSP27 antibody was conjugated with Au NPs as a targeted probe, photoacoustic microscopy enabled detection of the injured nerve [Fig. 7(c)]. The results indicate that Au NP-HSP27Abs can efficiently localize in the injured nerve and be detected by photoacoustic microscopy. Due to the low penetration depth of light in biological tissue and interference due to light absorption by muscle hemoglobin and surrounding blood vasculature, the morphology of the nerve could not be adequately observed using this method. However, these complications can be resolved by using a near-infrared (NIR) laser as the light source for photoacoustic microscopy in future studies. The obvious advantage of gold nanorods with a NIR laser for photoacoustic microscopy is the ability to circumvent the limitations of imaging depth and definition. Nevertheless, to our best knowledge, this is the first demonstration using Au NPs-HSP27Abs as a

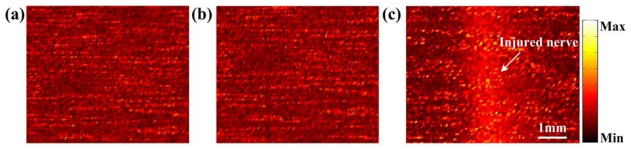

Fig. 7. *In vivo* photoacoustic microscopy of an Au NP-HSP27Ab-targeted injured nerve. Nontargeting Au NPs or targeting Au NP-HSP27Abs (100 μL, 8 mmol/L) were injected to a normal or injured nerve *in situ* before imaging. (a) Image of a normal nerve following Au NP-HSP27Ab injection. (b) Image of an injured nerve 7 days after injury and injected with Au NPs. (c) Image of injured nerve 7 days after injury and injected with Au NPs-HSP27Ab.

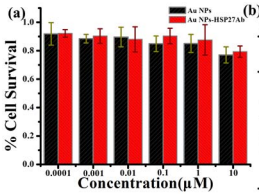

(b) The rat serum level of biochemical variables at 3 and 7 days after intravenous treatment with Au NPs-HSP27Ab (200μl/mouse).

Parameters	Saline (7 days)	GNRs-HSP27 (3 days)	GNRs-HSP27 (7 days)
Creatinine(mg/dl)	51.3±7.6	68.2±10.3	62.5±8.6
Alkaline phosphatase(U/L)	168.4±32.5	176.3±23.4	154.3±63.2
ALT(U/L)	56.3±7.8	66.7±10.2	64.4±9.8
AST(U/L)	220.7±19.8	196.5±23.4	232.5±13.2
LDH(U/L)	1314.2±58.4	1123.1±72.5	1264.3±56.2
BUN(mg/dl)	10.2±1.2	9.6±0.9	10.1±1.6
GGT（U/L）	3.2±0.6	3.4±0.8	2.8±1.1

Fig. 8. (a) Viability of HL-7702 cells exposed to different concentrations of GNRs or GNRs-HSP27Abs. The data are plotted as the percentage of viable cells compared to untreated controls. (b) The serum levels of biochemical variables in rats at 3 and 7 days. Values are means +/− SD (ratio to control), $n = 3$. There were no significant differences in any of the above parameters between the GNRs-HSP27Abs group and saline controls ($p > 0.05$). BUN, blood urea nitrogen; AST, aspartate aminotransferase; ALT, serum alanine aminotransferase; LDH, lactate dehydrogenase.

nanotargeting probe for photoacoustic microscopy to detect injured nerves. Taken together, our results demonstrate that Au NPs-HSP27Abs can be detected in injured nerves by photoacoustic microscopy.

Biocompatibility has been an important issue for *in vivo* applications of NPs. The results from analyses of Au NPs-HSP27Abs biocompatibility include *in vitro* cell toxicity and *in vivo* blood biochemistry analyses. HL-7702 cells were exposed to Au NPs and Au NPs-HSP27Abs continuously at different concentrations for 48 h and were measured by CCK-8 assay. Viability estimation showed no obvious toxic effect of Au NPs-HSP27Abs on HL-7702 cells [Fig. 8(a)]. Following tail vein injection of Au NPs-HSP27Abs (200 μL/rat, 1 μmol/L), there were no significant differences in any serum biochemical parameters between the rats treated with AU NPs-HSP27Abs and those treated with saline 3 and 7 days after intravenous injections [Fig. 8(b)]. In our study, toxicity test results revealed that a single imaging dose of Au NPs or Au NPs-HSP27Abs provided appropriate biocompatibility and satisfactory biosafety.

In conclusion, we use Au NPs-HSP27Abs as a new molecular imaging nanotargeting probe for photoacoustic microscopy to detect a nerve injury *in vitro*. Expression of HSP27 is significantly increased and localized throughout the bundle of the crush-injured sciatic nerve. By combining HSP27Ab (a targeting molecule) with Au NPs (a molecular carrier), an effective nanotargeting Au NPs-HSP27Abs probe is successfully constructed. Injured neurons dramatically increase the uptake of Au NPs-HSP27Abs. *In vitro* experiments demonstrate that injured nerves targeted with the Au NPs-HSP27Abs probe can be imaged by photoacoustic microscopy *in vitro* sciatic nerve injury. The results show the promise of HSP27Ab conjugated to Au NPs as novel nanotargeting probes for use in photoacoustic microscopy to detect early stage nerve injury.

This work was supported by the National Natural Science Foundation of China (No. 81271619), the

Natural Science Foundation of Guangdong Province (No. 10151503102000016), the National High Technology Research and Development Program of China (No. 2015AA020901), the Science and Technology Planning Project of Guangdong Province (No. 2013B090500122), and the Guangdong Natural Science Foundation (No. S2013020012646).

References

1. R. N. Kalaria, Nutr. Rev. **68**, S74 (2010).
2. W. W. Campbell, Clin. Neurophysiol. **119**, 1951 (2008).
3. A. V. Korompilias, A. H. Payatakes, A. E. Beris, M. D. Vekris, G. D. Afendras, and P. N. Soucacos, J. Microsurg. **26**, 288 (2006).
4. J. Zhu, F. Liu, D. Li, J. Shao, and B. Hu, Eur. J. Radiol. **21**, 1097 (2011).
5. D. D. Linda, S. Harish, B. G. Stewart, K. Finlay, N. Parasu, and R. P. Rebello, RG **30**, 1373 (2010).
6. W. S. Cho, M. Cho, J. Jeong, M. Choi, H. Y. Cho, B. S. Han, S. H. Kim, H. O. Kim, Y. T. Lim, and B. H. Chung, Toxicol. Appl. Pharmacol. **236**, 16 (2009).
7. H. Qin, T. Zhou, S. Yang, Q. Chen, and D. Xing, Nanomedicine (Lond) **8**, 1611 (2013).
8. M. Prato, K. Kostarelos, and A. Bianco, Acc. Chem. Res. **41**, 60 (2008).
9. S. K. Sahoo, S. Parveen, and J. J. Panda, Nanomedicine **3**, 20 (2007).
10. J. Zhang, S. Yang, X. Ji, Q. Zhou, and D. Xing, J. Am. Coll. Cardiol. **64**, 385 (2014).
11. B. Li, H. Qin, S. Yang, and D. Xing, Opt. Express **22**, 20130 (2014).
12. Y. Wang, J. Yuan, S. Du, X. Liu, G. Xu, and X. Wang, Chin. Opt. Lett. **13**, 061001 (2015).
13. Z. Wu, M. Sun, Q. Wang, T. Liu, N. Feng, J. Liu, and Y. Shen, Chin. Opt. Lett. **12**, 121701 (2014).
14. Z. Chen, S. Yang, and D. Xing, Opt. Lett. **37**, 3414 (2012).
15. S. Yang, F. Ye, and D. Xing, Opt. Express **20**, 10370 (2012).
16. S. Yang, D. Xing, Q. Zhou, L. Xiang, and Y. Lao, Med. Phys. **34**, 3294 (2007).
17. G. Liu and Z. Chen, Chin. Opt. Lett. **11**, 11702 (2013).
18. P. Mehlen, C. Kretz-Remy, X. Preville, and A. P. Arrigo, EMBO J. **15**, 2695 (1996).
19. J. N. Lavoie, G. Gingras-Breton, R. M. Tanguay, and J. Landry, J. Biol. Chem. **268**, 3420 (1993).
20. M. Costigan, R. J. Mannion, G. Kendall, S. E. Lewis, J. A. Campagna, R. E. Coggeshall, J. Meridith-Middleton, S. Tate, and C. J. Woolf, J. Neurosci. **18**, 5891 (1998).
21. K. Hirata, J. He, Y. Hirakawa, W. Liu, S. Wang, and M. Kawabuchi, Glia **42**, 1 (2003).